2024

Quantum spin glasses.

Quantum spin glasses are a fascinating class of materials where interactions between spins are so frustrated that no simple magnetic order can form. Understanding the nature of these materials is a challenging problem. Unlike regular magnets, spin glasses feature randomly arranged spins that freeze into unpredictable orientations at low temperatures causing a unique energy landscape with numerous local minima. Spin glass systems display a phase transition characterized by the breaking of a complex symmetry known as replica symmetry. The order parameters are defined as the overlaps between different replicas. Unlike conventional magnets, the transition in spin glasses is typically not sharp, which complicates the experimental observation of both the glass transition and the associated glassy properties. Consequently, there is a significant need for theoretical studies of spin glass models. Spin glasses are scientifically relevant not only in condensed matter physics but also in interdisciplinary fields. They provide insights into neural networks, optimization problems, and even economics. The mathematical techniques developed to understand spin glasses have found correspondence with problems in computer science, such as the study of algorithmic complexity and information theory.

Classical spin glasses have been investigated extensively, and much progress has been achieved through the exact solution of mean-field models such as the famous classical Sherrington-Kirkpatrick (SK) model which is an Ising model with long-range frustrated ferromagnetic (which align spins in the same direction) and antiferromagnetic (which align spins in opposite directions) couplings. The simplest possible extension that adds quantum-mechanical aspects to the SK model is the inclusion of a transverse magnetic field, which adds additional layers of complexity. By combining the advanced continuous-time quantum Monte Carlo numerical technique with the sophisticated mathematical method of replica symmetry breaking we construct a numerically exact solution to this model [1].

Our study reveals the complete phase diagram of the model with a quantum glass phase at low temperatures and transverse fields, which is shown in Figure 1.A. Both thermal and quantum fluctuations melt the glass phase leading to the emergence of the paramagnetic phase. The quantum spin glass features non-trivial spin dynamics which we are able to compute with great detail. We determine the dynamical response of the spins, as well as their static response functions. We also extracted the distribution of the order parameters that characterizes how spins are correlated in the spin glass phase. Importantly, we derive the precise form of the dynamical response function which reflects the presence of abundant low-energy excitations. We find that the low-energy part of the response function is highly insensitive to the value of the transverse magnetic field in the glassy phase (Figure 1.B). This property is compared to the results with experimental measurements performed on the rare-earth compound $LiHo_xY_{1-x}F_4$ in a transverse field, which is believed to undergo a quantum spin glass transition [2]. We find an excellent agreement between our mean-field results and the experimental data., highlighted in Figure 1.B.

In summary, we advance the theoretical understanding of quantum spin glasses, bridging the gap between theoretical models and experimental results. Our work provides a general framework for solving other mean-field quantum glass models such as electron glasses and quantum Heisenberg spin glasses.

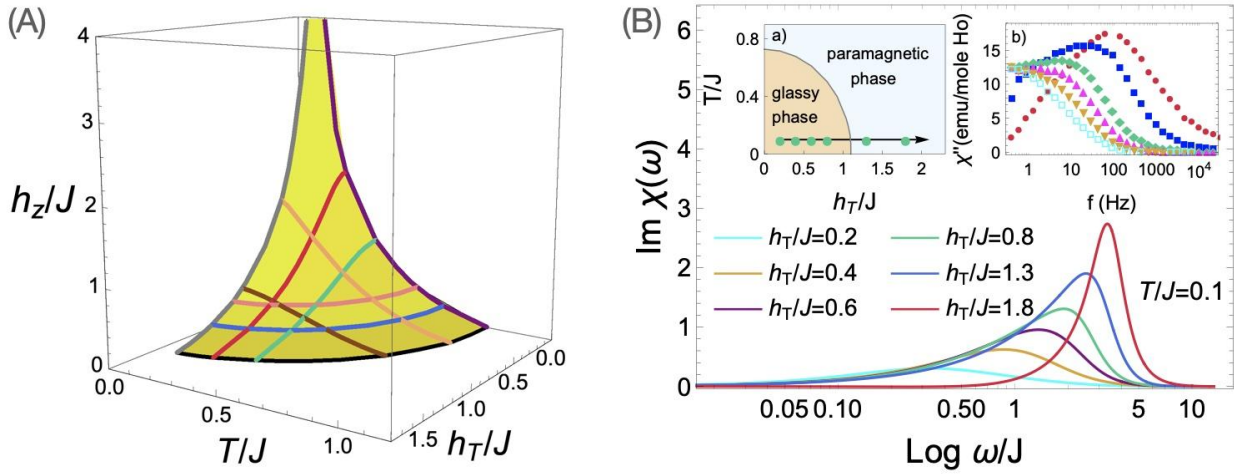

Figure 1. (A) Phase diagram in terms of the temperature T, transverse field h_T, and on-site disorder h_z, measured in units of the interaction strength J. (B) Comparison between the calculated dynamical susceptibility (main panel) and a.c. susceptibility measurements [2] (panel b)) moving from the spin glass phase to the paramagnetic phase as indicated in panel a) by varying the value of the transverse magnetic field.

References:

[1] A. Kiss, G. Zaránd and I. Lovas, *Complete replica solution for the transverse field Sherrington-Kirkpatrick spin glass model with continuous-time quantum Monte Carlo method*, Phys. Rev. B 109, 024431 (2024) https://doi.org/10.1103/PhysRevB.109.024431

[2] C. Ancona-Torres, D. M. Silevitch, G. Aeppli, T. F. Rosenbaum, *Quantum and classical glass transition in* $LiHo_xY_{1-x}F_4$, Phys. Rev. Lett. 101, 057201 (2008) https://doi.org/10.1103/PhysRevLett.101.057201

2023

Shiba band structure and topological edge states of artificial spin chains.

In recent years there is an intense race to detect Majorana Zero Modes (MZMs), that could provide a unique platform for fault-tolerant quantum computing,the real breakthrough - that has created a great number of routes to such platforms - was the realization that one can create topological superconductivity based on artificial heterostructures. However, MZMs in superconducting heterostructures are still elusive because it is very difficult to uniquely identify them experimentally. Several promising STM experiments have been performed on various systems, which show peaks in the differential conductivity at zero energy in the superconducting gap of the host. However, this does not impose a strict evidence that the observed states at the end of the chain are indeed the long sought MZMs and further information about the nature of these peaks are difficult to obtain. At the same time, most theoretical models which claim to calculate Majoranas are able to do so only if unrealistic parameters are used, which, for example, gives rise to an enormous superconducting gap. To address this problem we developed a first-principles based, hence parameter less computational approach by solving of the Kohn-Sham-Dirac-Bogoliubov de Gennes (KSDBdG) equations. Such an approach can not only reproduce many aspects of the STM experiments, as we demonstrated earlier, but it also allows the calculation of other quantities, like spin-polarization and the superconducting order parameter (OP), which are important to understand the nature of these states, but are not easily accessible to experiments. Furthermore, some of their properties can be further explored and tested by computational experiments which are also beyond the capabilities of conventional experimental techniques. Therefore we performed first principles calculations in the superconducting state for Fe chains on Nb(110) hosts with a single Au overlayer, where relativity, superconductivity and the complex geometry and electronic structure is treated on the same level. Additionally within our Green’s function based approach it can be done without the introduction of a supercell.

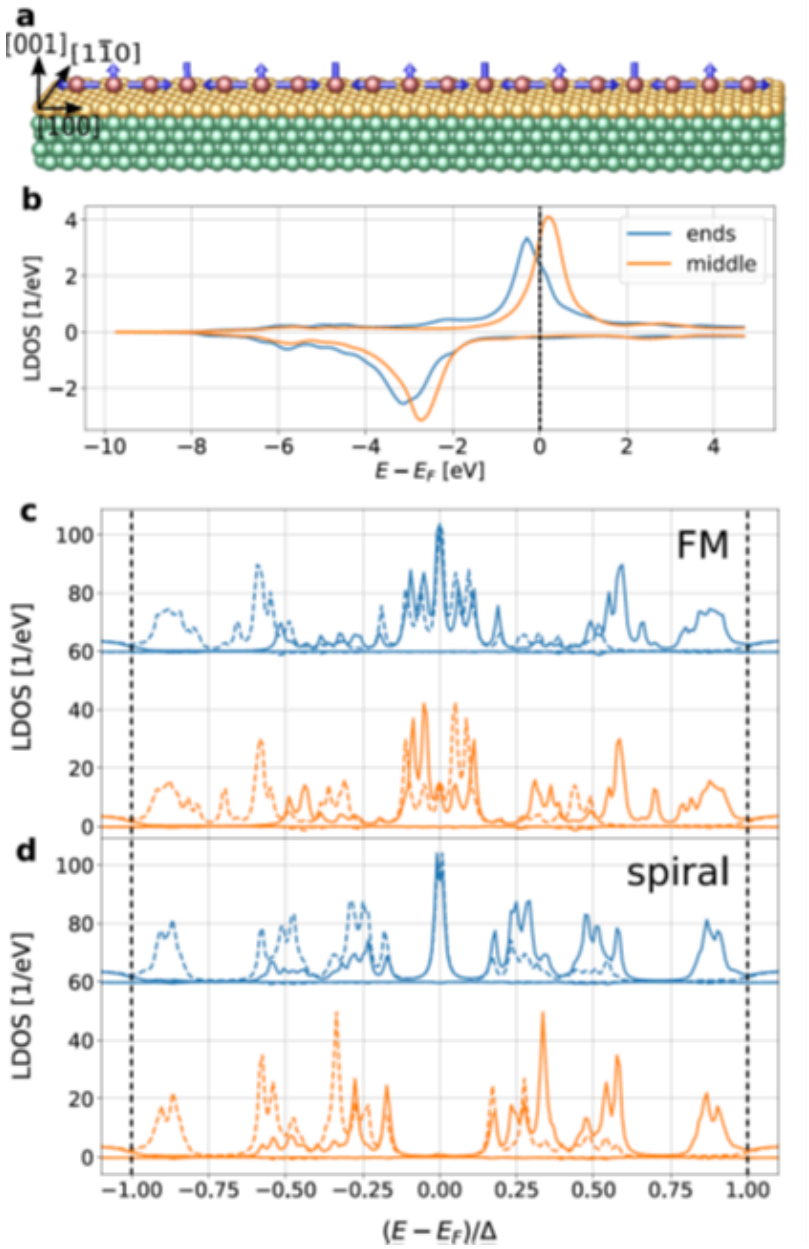

Figure 1 The Local Density od States (LDOS) of the 2a-[100] Fe19 chain on Au/Nb(110) in the normal and in the superconducting state. (a), the illustration of a Fe chain on Nb(110) covered with a single monolayer Au, the spin configuration shows a Néel spiral with 90° spiraling angle. (b) the normal state local density of state for the ferromagnetic chain. (c) the LDOS in the superconducting state of the ferromagnetic chain. (d) the LDOS of the same chain as in (c) but in a 90° Néel spiral The blue curves are calculated on the first atom of the chain and the orange are from the middle of the chain. The black dashed vertical lines in panel (c) and (d) indicate the superconducting gap of the Nb, Delta=1.51 meV.

On Fig. 1 it can be seen that in the magnetic chain the Yu-Shiba-Rusinov (YSR) states of the single Fe impurity hybridize within the superconducting gap of the host, as it was seen in the experiments, and the hybridized states occupy almost the entire energy range of the gap, including the vicinity of zero energy. Most interestingly however, when repeating the calculation for a 90° Néel type spin spiral, the LDOS plotted in Fig.1d shows the opening of an internal gap of Δ=0.22 meV around zero energy within the hybridized YSR states. Moreover, one peak remains seemingly untouched right in the middle of this mini gap, exactly at zero energy - that is, at the Fermi energy - on the atoms at both ends of the chain. In connection to STM experiments, these peaks at zero energy are often referred to as Zero Bias Peaks (ZBPs). It is expected, that that MZMs appear at the two ends of the chains.

We visualize our results for a wide range of spirals on in Fig, 2 by plotting the DOS (LDOS summed over all atoms in a chain) obtained for many different spirals as a function of the spiraling rotation angle .

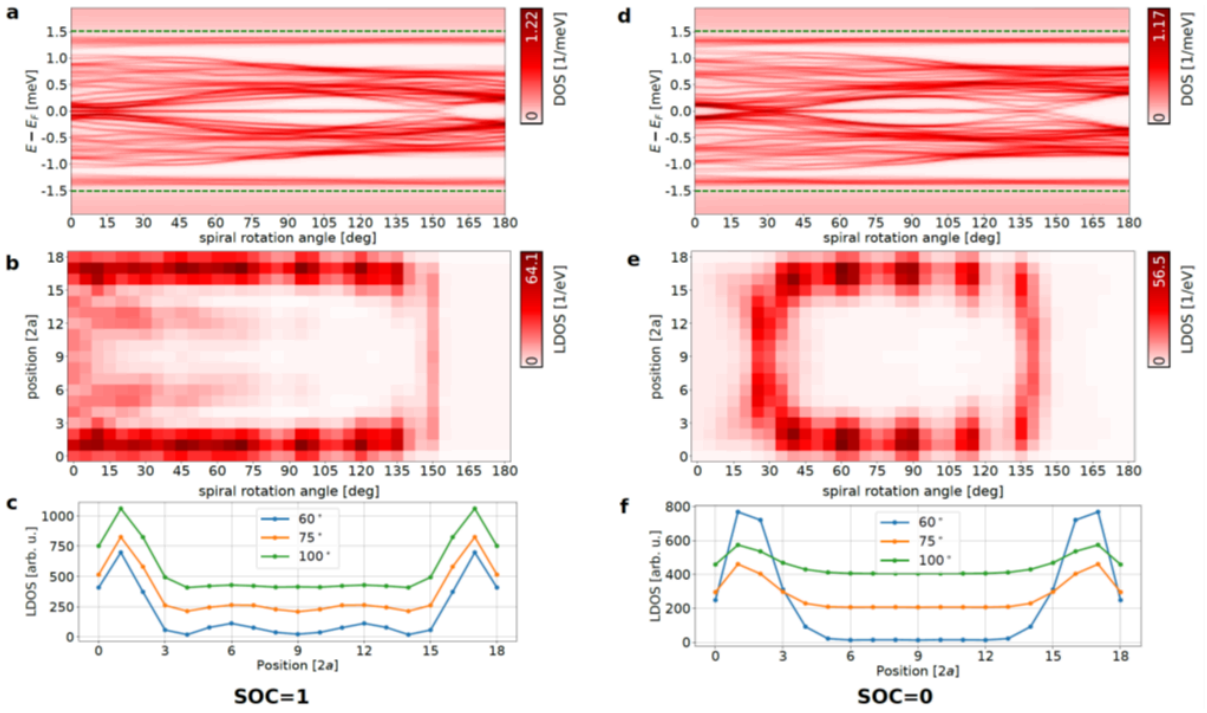

Figure 2 The effect of the SOC on the DOS, and the localization of the ZEP of Néel spirals for the Fe192a-[100] chains on Au/Nb(110). (a), the total DOS, integrated along the chain plotted in the vicinity of the superconducting gap (1.51 meV), noted with green dashed lines. Calculated for Néel spirals with rotations angles changed in 5° steps between the ferromagnetic 0° and the antiferromagnetic 180° spin configurations, in the fully relativistic case, noted as SOC=1. (b) the electron LDOS at the Fermi energy along the 2a-[100] Fe19 chain on Au/Nb(110) as a function of the Néel spiral rotation angle in the fully relativistic case SOC=1. (d) and (e) are the same as (a) and (b), but with SOC scaled to 0. In panels (c) and (f) different cross sections are shown from (b) and (e) respectively, in order to better show the localization of the states, the lines are plotted with an offset of 200 arb. units.

One can easily see on Fig. 2a, that there is no meaningful gap present for the FM case. However as the spiraling angle is increasing, a minigap opens and starts to increase in size from about 20°, and keeps increasing until around 110°, where it reaches its maximum value of 0.25 meV which is 16.5 % of the full Nb gap. For larger spiraling angles the minigap starts to decrease and it collapses at around 150° and then reopens again. Probably, the most interesting feature of Fig. 2a is the existence of a state at zero energy. This state is present even in the FM state - just there is no gap around it - and remains undisturbed while the minigap opens all the way until the minigap closes again at 150° and disappears as the gap reopens for even larger spiraling angles. In order to investigate the dependence of both the minigap and the ZBP on Spin-Orbit Coupling (SOC), we repeated our calculations with SOC scaled out from the KSDBdG equations. The results can be analyzed by comparing Fig. 2a and d. Calculations behind these figures are completely identical otherwise. Probably, the most prominent effect is, that without SOC the ferromagnetic state is gapped without a ZBP in it. On Fig, 2b, c, e, and f, one may observe the spatial extent of the Majorana state. The frequently assumed physical picture is that the larger coherence length (smaller gap sizes) will be much more likely to cause larger localization length and thus hybridization of MZMs. The results we obtained here significantly changes this picture emphasizing the importance of spin-orbit effects and the necessity of a material specific treatment.

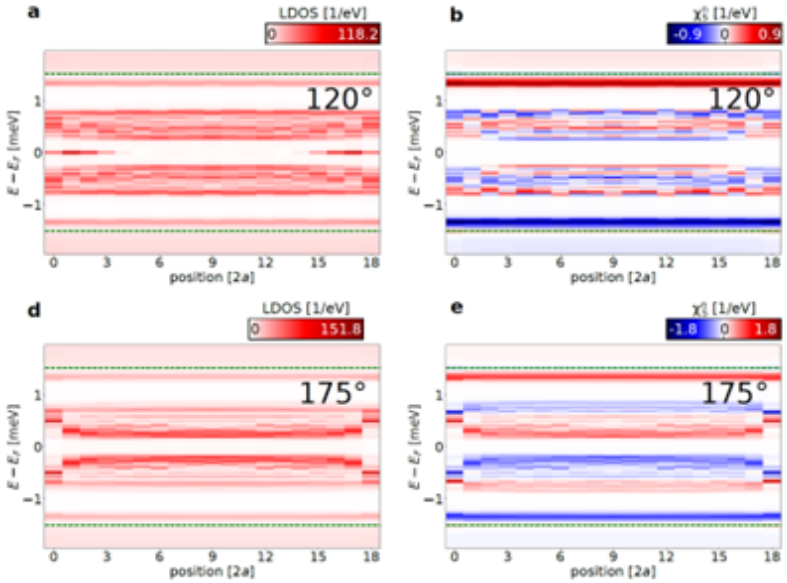

Figure 3The real space structure of the LDOS and the energy-resolved singlet OP in the presence and in the absence of a {ZEP}.

One may assign band inversion as a key signature of a topological system, which is than typically observed in the band structure of infinite systems. At the same time, in addition to the electron (and hole) densities, the KSDBdG equations also provides us with a recipe to calculate the singlet OPs. We found that in the superconducting state, band inversion may be indicated by the energy-resolved singlet OP, due to its antisymmetric property with respect to the Fermi level, even in the case of a finite chain. This can be seen in Fig. 3, where the singlet OP is plotted along with the LDOS in the presence and absence of an MZM. It is easily observable that while in the case of a 170° spiral, where no ZBP is present, the sign of the singlet OP is the same at the positive (negative) energy edge of the minigap and the positive (negative) energy edge of the superconducting gap. However, for a 100° spiral this changes around so, that the sign of the OP is opposite at the minigap edges than at the coherence peaks at superconducting gap. This we found to be an indication of band inversion, and, consequently, a topological minigap.

References:

[1] DOI: https://doi.org/10.1038/s42005-023-01196-y
[2] DOI: https://doi.org/10.1103/PhysRevB.108.134512
[3] DOI: https://doi.org/10.1103/PhysRevB.108.134513

In 2023, our research group has made further substantial steps towards developing elementary hardware elements for quantum information processing. These elements are solid-state quantum bits, in most cases point defects which show magneto-optical behavior which can be harnessed to store and process quantum information. A proper investigation of such systems include their precise physical description, as for both their actual molecular structure and electronic system properties, as well as proposing a set of so-called quantum protocols which make them really usable as quantum bits, and finally validating their fundamental chemical and engineering properties for the usage in real quantum information processing environments. In almost every case, these systems are also promising candidates for nanometrology (nanosensing, biosensing) applications, as the physics of these two fields are closely related. We executed ab initio calculations on modeling the qubits by KIFÜ high-performance computing units as well as our local high performance computation cluster.
Formation of G-center in silicon. Thermal equilibrium is reached when the system assumes its lowest energy. This can be hindered by kinetic reasons; however, it is a general assumption that the ground state can be eventually reached. Here, we show that this is not always necessarily the case. Carbon pairs in silicon have at least three different configurations, one of them (B-configuration) is the G photoluminescence center. Experiments revealed a bistable nature with the A-configuration (Fig. A). Electronic structure calculations predicted that the C-configuration is the real ground state; however, no experimental evidence was found for its existence. Our calculations show that the formation of the A- and B-configurations is strongly favored over the most stable C-configuration which cannot be realized in a detectable amount before the pair dissociates. Our results demonstrate that automatized search for complex defects consisting of only the thermodynamically most stable configurations may overlook key candidates for quantum technology applications.

Fig. A. A, B, and C label the three configurations identified in prior studies. Brown and blues spheres are the carbon and silicon atoms, respectively. The figures are made by Crystal MakerTM.

Diamond NV center spin-phonon interactions. Spin-lattice relaxation within the diamond nitrogen-vacancy (NV) center's electronic ground-state spin triplet limits its coherence times, and thereby impacts its performance in quantum applications. Our collaborators observed the relaxation rates on the NV center's $|ms=0\rangle \leftrightarrow |ms=\pm1\rangle$ and $|ms=-1\rangle \leftrightarrow |ms=+1\rangle$ transitions as a function of temperature from 9 to 474 K in high-purity samples. We showed that the temperature dependencies of the rates are reproduced by our ab initio theory of Raman scattering due to second-order spin-phonon interactions which is generally applicable to other defect spin systems [B]. We developed a theory about the nuclear spin relaxation under resonant excitation to polarize the 14N host, which our collaborator then prove beneficial for spin magnetometry in experiments [C]. The nuclear spin relaxation is mediated by the electron-phonon coupling in the electronic excited state according to our theory.
Diamond NV centers close to the surface.
Near-surface negatively charged nitrogen vacancy (NV) centers hold excellent promise for nanoscale magnetic imaging and quantum sensing. However, they often experience charge-state instabilities, leading to strongly reduced fluorescence and NV coherence time, which negatively impact magnetic imaging sensitivity. This occurs even more severely at 4 K and ultrahigh vacuum (UHV, p = 2 × 10–10 mbar). Our collaborators demonstrate that in situ adsorption of H_2O on the diamond surface allows the partial recovery of the shallow NV sensors. Our band-bending calculations showed that controlled surface treatments are essential for implementing NV-based quantum sensing protocols under cryogenic UHV conditions [D]. Molecules or ions with unpaired electronic spins are typically probed by their influence on the NV center's spin relaxation. Whereas it is well-known that paramagnetic ions reduce the NV center's relaxation time (T1), our collaborators reported on the opposite effect for diamagnetic ions. To elucidate the underlying mechanism of this surprising effect, single and double quantum NV experiments are performed, which indicate a reduction of magnetic and electric noise in the presence of diamagnetic electrolytes. Our ab initio simulations shows that a change in the interfacial band bending due to the formation of an electric double layer leads to a stabilization of fluctuating charges at the interface of an oxidized diamond [E].
Hexagonal boron nitride boron-vacancy spin's coupling to external fields. Hexagonal boron nitride (hBN) has recently been demonstrated to contain optically polarized and detected electron spins that can be utilized for implementing qubits and quantum sensors in nanolayered-devices. The boron-vacancy spin defect in hexagonal boron nitride (hBN) has a great potential as a quantum sensor in a two-dimensional material that can directly probe various external perturbations in atomic-scale proximity to the quantum sensing layer. Here, we apply first-principles calculations to determine the coupling of the electronic spin to strain and electric fields. Our work unraveled the interplay between local piezoelectric and elastic effects contributing to the final response to the electric fields. The theoretical predictions are then used to analyze optically detected magnetic resonance (ODMR) spectra recorded on hBN crystals containing different densities of centers. We prove that the orthorhombic zero-field splitting parameter results from local electric fields produced by surrounding charge defects [F]. These results explain the observations of boron-vacancy spin defects in few-atomic-layers thick hexagonal boron nitride [G].

References:
[A] https://www.nature.com/articles/s41467-023-36090-2
[B] https://journals.aps.org/prl/abstract/10.1103/PhysRevLett.130.256903
[C] https://journals.aps.org/prl/abstract/10.1103/PhysRevLett.131.236901
[D] https://pubs.acs.org/doi/10.1021/acs.nanolett.2c04733
[E] https://pubs.acs.org/doi/10.1021/acsnano.3c01298
[F] https://www.nature.com/articles/s41524-023-01111-7
[G] https://journals.aps.org/prl/abstract/10.1103/PhysRevLett.131.116902

2022

2D materials, 2D magnetic layers, and 2D molecular structures —

Two-dimensional (2D) few-atoms-thick materials are in the forefront of scientific research due to their intriguing properties and potential for diverse future technological applications. Recently, various stackings and combinations of 2D materials exhibited even more interesting and exploitable properties, and the research of such 2D material stacks is, presently, far from being complete. Our group contributed to gaining knowledge on 2D materials and their combinations, 2D (ultrathin) magnetic films, and 2D self-assembled molecular structures.
The most well known 2D material is graphene composed of carbon atoms in a honeycomb lattice, which is a gapless semiconductor, but a multitude of other materials are also under active research. One class of such 2D materials is the family of transition metal dichalcogenides (TMDCs), which usually exhibit semiconducting properties with non-zero gaps. Combining graphene with 2D TMDCs into so-called van der Waals heterostructures leads to the emergence of fascinating phenomena.

In the first example, trapped charges between graphene and $ReSe_2$ have been directly observed by scanning tunneling microscopy (STM) and spectroscopy (STS) experiments and density functional theory (DFT) calculations [1]. Interestingly, when measuring the STM topography within the band gap of $ReSe_2$, features resembling the $ReSe_2$ lattice rather than the graphene one are visible. Based on a theoretical analysis, it is found that electron accumulation appears just below the $ReSe_2$ layer and electron depletion occurs at the graphene side, resulting in an asymmetrically polarized electron density between the two 2D materials. It is also found that this so-called trapped charge is further accumulated at ReSe2 step edges. This work has been done in collaboration with Korean groups.

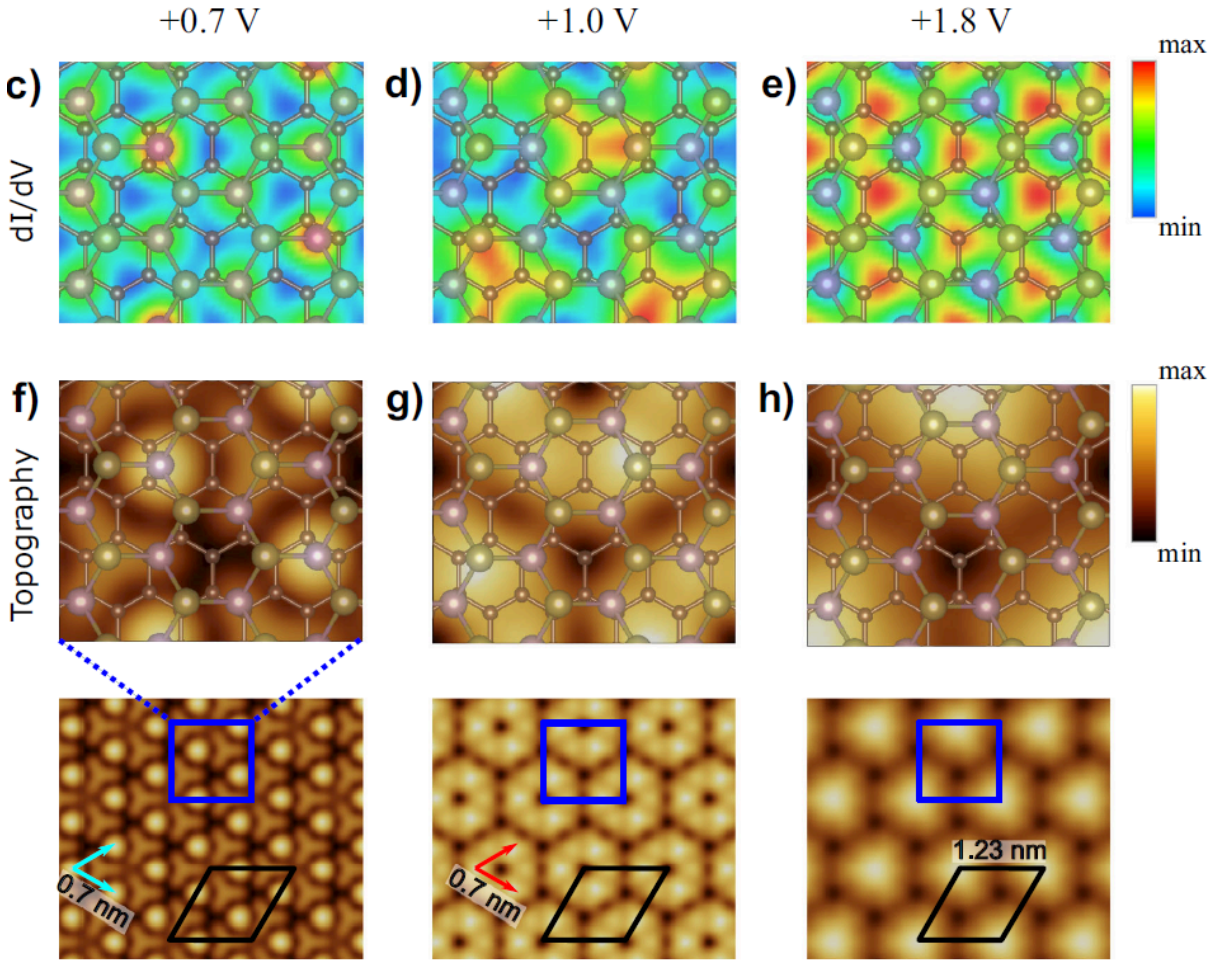

Figure 1. Calculated STS maps (dI/dV, top row) and STM topographies (bottom two rows) of various electronic Moiré patterns appearing at different bias voltages in a $MoTe_2$/graphene heterostructure [2].

In the second example, the combination of graphene and MoTe2 was studied by STM/STS measurements and DFT calculations [2]. It was found that the complex electronic structure of this van der Waals heterostructure exhibits unusually rich higher-indexed electronic Moiré patterns, which are extremely sensitive to the probing electron energy, or bias voltage in the STM junction (Fig. 1). A detailed theoretical analysis revealed the key energy-dependent electronic states contributing to the observed phenomena. Interestingly, the trapped charges are also present in this 2D heterojunction [2] just as in the previous example [1]. This work has been done in collaboration with the Centre for Energy Research and Belgian and French groups.

We also performed theoretical research in collaboration with experimentalists from Germany and Poland on ultrathin 2D magnetic films. The coexistence of antiferromagnetism (AFM) and proximity-induced superconductivity has been proved on a Mn atomic monolayer and bilayer on a Nb(110) superconducting substrate [3]. Our theoretical analysis revealed that a c(2x2) AFM state with out-of-plane spin moments is formed in the Mn atomic layer due to the dominating nearest-neighbor (intralayer) AFM isotropic exhange coupling of the Mn spin moments, and the spin moments of Mn in the two atomic layers of the bilayer are also strongly (interlayer) AFM coupled. In another work, the magnetic states and the tuning of the magnetic transition temperature of an Fe atomic layer in a Au/Fe/Au/W(110) sandwich structure depending on the Au coverage was investigated [4]. Considering several structural models, our theoretical analysis mostly revealed ferromagnetic ground states for the Fe atomic layer with increased Fe spin moments upon Au coverage, and the calculated Curie temperature values are in fair agreement with those obtained from experiments. Furthermore, the presence of frustrated isotropic Fe-Fe exchange coupling was pointed out, and a discussion of the structural effects on the magnetic properties of Fe was provided.

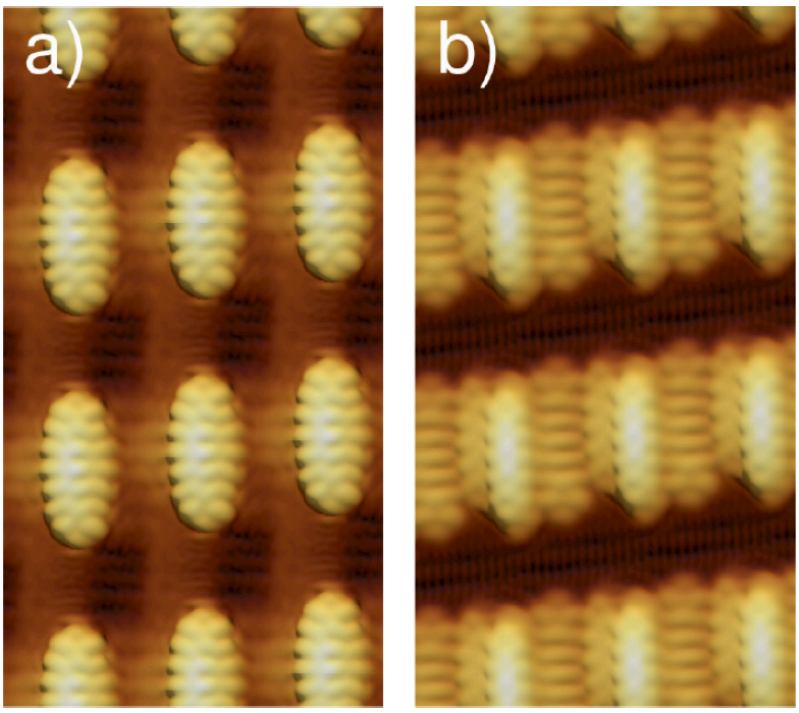

Figure 2. Calculated filled-state STM topographies of 2D pentacene molecular networks on the Si(553)-Pb surface: a) low-density phase: 1 pentacene/surface cell, b) high-density phase: 3 pentacenes/surface cell [5].

To extend research on 2D materials toward 2D patterns, 2D self-assembled molecular structures were studied by STM and DFT in collaboration with Polish groups. As a realization of such 2D molecular structures, the pentacene adsorption on the Si(553)-Pb surface has been considered [5], exhibiting a template-driven self-assembly depending on the molecular coverage. The experimentally observed molecular networks were identified by DFT and subsequent STM calculations (Fig. 2), where the subtle balance between the molecule-substrate and molecule-molecule interactions was also highlighted.

References:
[1] DOI: https://doi.org/10.1016/j.apsusc.2021.152187
[2] DOI: https://doi.org/10.1038/s41699-022-00321-9
[3] DOI: https://doi.org/10.1103/PhysRevB.105.L100406
[4] DOI: https://doi.org/10.3390/ma15031019
[5] DOI: https://doi.org/10.1021/acs.jpcc.2c05308
[6] DOI: https://doi.org/10.1140/epjp/s13360-022-03068-w

2021

Relativistic first-principles theory of Yu-Shiba-Rusinov states applied to Mn adatoms and Mn dimers on Nb(110) - Local magnetic moments inside or at surfaces of metals in the superconducting state lead to the formation of localized bound states within the superconducting gap, referred to as Yu-Shiba-Rusinov (YSR) states. The magnetic moment of an adatom is exchange-coupled to the Cooper pairs, and, due to the reduced symmetry of the crystal field of the substrate, several particle-hole symmetric pairs of YSR states are predicted within the gap.

Recently, we developed a first-principles material-specific description of YSR states where relativity, superconductivity, magnetism, and the entire host electronic structure are treated on the same footing [1]. We achieve this by solving the fully relativistic Bogoliubov–de Gennes equations via band-theoretical methods for the entire host-embedded impurity system.

The method is used to make a direct comparison with the most recent experiments for Mn adatoms on Nb(110) [2] (for some theoretical results, see Fig. 1). Furthermore, one immediately gains a deeper insight into the formation of the YSR states by artificially manipulating the exchange field of the impurity, the spin-orbit coupling, and the induced moments. We find that the spin-orbit coupling slightly shifts some of the YSR peaks and also the local spin-polarization on the Nb atoms has marginal effects to their positions. Moreover, by scaling the exchange field on the Mn site we could explain the lack of the YSR state in the spectrum.

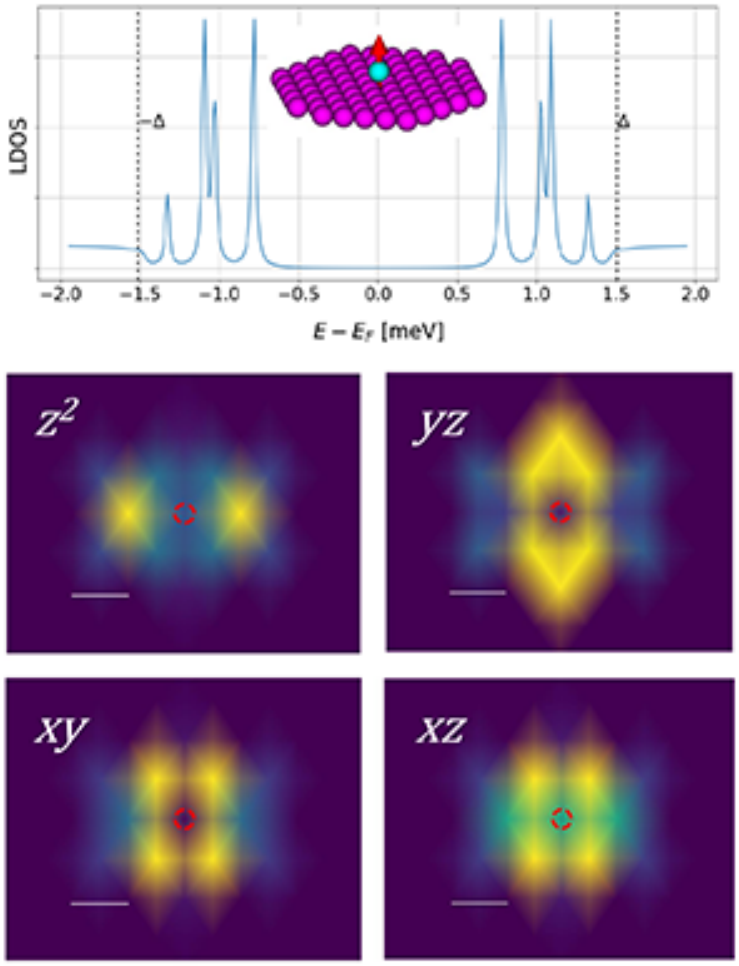

Figure 1. Local density of states of Mn adatom on Nb(110), and the color map of the local density of states in the vacuum layer containing the Mn adatom at the energies corresponding to the four YSR states identified in. The position of the Mn atom is marked by a small red circle. See [1] for more details.

Comparison with experiments is extended to Mn dimers, where we discuss the hybridization of the YSR states for dimers along different crystallographic directions. While our results for a close packed ferromagnetic dimer are in satisfactory agreement with the experimentally observed splitting of the YSR states, in case of an antiferromagnetic dimer we find that the spin-orbit coupling is not sufficiently large to explain the splitting of the YSR states seen in the experiment. Changing the relative orientation of the magnetic moments in this dimer induces splitting of the YSR states and also shifts their energy, leading even to the formation of a zero-bias peak. Our results strongly underlines the importance of such first-principles calculations for the interpretation of future experiments on longer chains and on other nanostructures with a zero-bias peak.

High Entropy Alloys - (HEAs) consist of several elements mixed in relatively large proportions, and the phase stability is controlled by the high entropy of mixing in combination with sluggish diffusion. HEAs are promising for application in transport, construction, aerospace and energy sectors, where high operating temperature, low density, and specific magnetic properties are required. However, practical implementation for magnetocaloric engineering requires the development of innovative materials, having excellent structural, mechanical and magnetic properties.

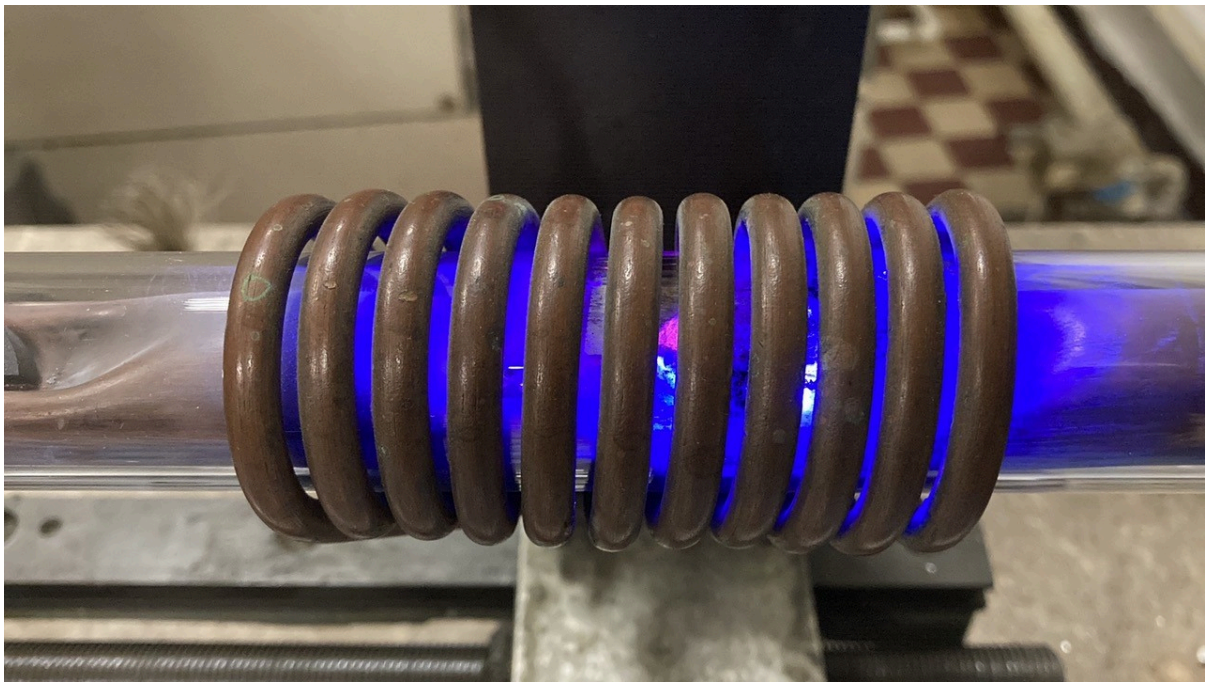

Figure 2 A High Entropy alloy int he making

Ab initio electronic structure calculations of the phase stability and magnetic transition temperature of AlxCr0.25MnFeCo0.25-yNiy alloys were performed to screen for compositions showing promising magnetocaloric properties in the vicinity of room temperature [3]. This theory-assisted alloy development approach is intended to contribute to the success of designing magnetic refrigerators for room-temperature applications. Magnetocaloric application for a series of MnxCr0.3Fe0.5Co0.2Ni0.5Al0.3 HEAs were explored by integrated theoretical and experimental methods [4]. Both theory and experiment indicate the designed HEAs have the Curie temperature close to room temperature and is tunable with Mn concentration. It is pointed out that improved magnetocaloric properties could be achieved by tuning Mn concentration.

In-situ switching between antiferromagnetic domains in the multiferroic $Ba_2CoGe_2O_7$ — The interaction between light and matter may produce fascinating phenomena. Among them is the nonreciprocal directional dichroism (NDD), when the absorption differs for the propagation of light along and opposite to a specific direction. The origin of this phenomenon is the chirality of the light, as the electric and magnetic field components of the light and its propagation vector form a right-handed system. NDD appears naturally in magnetoelectric multiferroics with coexisting orthogonal electric and magnetic orders. In [5], we demonstrated the in situ electric control of the population of antiferromagnetic domains in $Ba_2CoGe_2O_7$ using external magnetic and electric fields by analyzing the NDD response.

[1] B. Nyári, A. Lászlóffy, L. Szunyog, G. Csere, K. Park, B. Újfalussy: Relativistic first-principles theory of Yu-Shiba-Rusinov states applied to Mn adatoms and Mn dimers on Nb(110), Phys. Rev. B 104: 235426 (2021).

[2] P. Beck, L. Schneider, L. Rózsa, K. Palotás, A. Lászlóffy, L. Szunyogh, J. Wiebe, R. Wiesendanger, Spin-orbit coupling induced splitting of Yu-Shiba-Rusinov states in antiferromagnetic dimers, Nature Communications 12: 2040 (2021).

[3] S. Huang, Z. Dong, W. Mu, V. Strom, G. Chai, L. K. Varga, O. Eriksson, and L. Vitos: Magnetocaloric properties of melt-spun MnFe-rich high-entropy alloy, Appl. Phys. Lett. 119: 141909 (2021).

[4] Z. Dong, S. Huang, V. Strom, G. Chai, L. K. Varga, O. Eriksson, L. Vitos: MnxCr0.3Fe0.5Co0.2Ni0.5Al0.3 high entropy alloys for magnetocaloric refrigeration near room temperature, Journal of Materials Science & Technology 79: 15 (2021).

[5] J. Vít, J. Viirok, L. Peedu, T. Rõõm, U. Nagel, V. Kocsis, Y. Tokunaga, Y. Taguchi, Y. Tokura, I. Kézsmárki, P. Balla, K. Penc, J. Romhányi, S. Bordács: Terahertz detection of in-situ switching between antiferromagnetic domains in the multiferroic Ba2CoGe2O7, Phys. Rev. Lett. 127: 157201 (2021).

[6] D. Vörös, K. Penc: Dynamical structure factor of the SU(3) Heisenberg chain: Variational Monte Carlo approach, Phys. Rev. B 104: 184426 (2021).

[7] A. Thomasen, K. Penc, N. Shannon, J. Romhányi: Fragility of Z2 topological invariant characterizing triplet excitations in a bilayer kagome magnet, Phys. Rev. B 104: 104412 (2021).

[8] Z. Dong, W. Li, S. Schonecker, B. Jiang, and L. Vitos: Invariant plastic deformation mechanism in paramagnetic nickel-iron alloys, Proceedings of the National Academy of Sciences PNAS 118: e2023181118 (2021).

[9] Z. Yang, S. Lu, Y. Tian, Z. Gu, H. Mao, J. Sun and L. Vitos: Assessing the magnetic order dependent γ-surface of Cr-Co-Ni alloys, Journal of Materials Science & Technology 80: 66 (2021).

[10] S. Huang, Z. Dong, E. Dastanpour, V. Strom, G. Chai, V. K. Lajos, O. Eriksson, L. Vitos: Vibrational entropy-enhanced magnetocaloric effect in Mn-rich high-entropy alloys, Applied Physics Letters 119: 084102 (2021).

[11] G. Qin, R. Chen, H. Mao, Y. Yan, X. Li, S. Schonecker, L. Vitos, X. Li: Experimental and theoretical investigations on the phase stability and mechanical properties of Cr7Mn25Co9Ni23Cu36 high-entropy alloy, Acta Materialia 208: 116763 (2021).

[12] Z. Yang, J. S., S.Lu, and L. Vitos: A comparative study of solid-solution strengthening in Cr-Co-Ni complex concentrated alloys: The effect of magnetism, Computational Materials Science 192: 110408 (2021).

[13] L-Y. Tian, O. Guteisch, O. Eriksson, L. Vitos: Alloying effect on the order-disorder transformation in tetragonal FeNi, Scientific Reports 11: 5253 (2021).

[14] Z. Dong, W. Li, B. Jiang, Q. Li, F. Pan, and L. Vitos: Thermo-mechanical properties of Cr-Co-Ni alloys from longitudinal spin fluctuation theory, Appl. Phys. Lett. 119: 081904 (2021).

[15] A. Lászlóffy, K. Palotás, L. Rózsa, and L. Szunyogh: Electronic and magnetic properties of building blocks of Mn and Fe atomic chains on Nb(110), Nanomaterials 11: 1933 (2021).

[16] K. Palotás, L. Rózsa, E. Simon, and L. Szunyogh: High-resolution tunneling spin transport characteristics of topologically distinct magnetic skyrmionic textures from theoretical calculations, Journal of Magnetism and Magnetic Materials 519: 167440 (2021).

[17] Y.-J. Lee, T. T. Ly, T. Lee, K. Palotás, S. Y. Jeong, J. Kim, and A. Soon: Completing the picture of initial oxidation on copper, Applied Surface Science 562: 150148 (2021).

[18] T. Ossowski, T. Pabisiak, A. Kiejna, K. Palotás, and E. Bauer: Simulation of STM images of hematite α-Fe2O3(0001) surfaces: Dependence on distance and bias, Journal of Physical Chemistry C 125:, 26711 (2021).

[19] K. Niu, X. Ni, H. Wang, Y. Li, K. Palotás, H. Lin, and L. Chi: On-surface synthesis of 2D COFs via molecular assembly directed photocycloadditions: A first-principles investigation, Journal of Physics: Condensed Matter 33: 475201 (2021).

2020

Spin transport on magnetic skyrmions — Magnetic skyrmions are real-space non-collinear spin structures with intriguing properties and they are promising building blocks for high-density information storage and low-power information carrier applications in spintronics due to their small size and topological properties. They are formed of closed magnetic domain walls of diverse complexity in real space, and are characterized by topological

invariants. The winding number or topological charge of the three-dimensional spin vectors is the most commonly used quantity. There are several challenges to overcome to be able to use these objects in real device applications: room temperature stability, controlled writing, reading and deleting, moving them by electric currents or other ways, all-electrical detection and manipulation, switching their topological properties, etc. First-principles calculations provide deep insight into the role of antisymmetric Dzyaloshinsky-Moriya, isotropic Heisenberg and symmetric anisotropic magnetic exchange interactions, exchange frustration, higher-order magnetic interactions, and magnetocrystalline anisotropy in the formation of skyrmions in thin magnetic films. Tailoring their dynamical properties requires an advanced understanding of their spin transport, spin dynamics and spin switching properties. Due to their small size a viable route to controllably manipulate their spins is through locally focused perturbations, like laser beams, or scanning probe methods.

Spin-polarized scanning tunneling microscopy (SP-STM) has been extensively used to image (with atomic resolution) and manipulate magnetic skyrmions and other complex magnetic objects at surfaces thanks to atomically sharp scanning tips. The controlled creation and annihilation of skyrmions have been demonstrated by using local current pulses of the tip of an STM with opposite voltage polarities. These effects have been explained by the electric fields in the STM junction, but the roles of the tunneling spin transfer torque (STT) and other spin transport processes in an SP-STM, where the spin-polarized current exerts a torque on the spin moments of the sample, are less understood. This motivated our very recent work [1], where the tunneling electron spin transport properties of six topologically distinct magnetic skyrmions in an ultrathin film were investigated based on theoretical calculations. An electron tunneling theory for the combined calculation of scalar charge and vector spin transport in SP-STM within the three-dimensional Wentzel-Kramers-Brillouin framework was utilized. The topologies of the maps of the calculated tunneling vector spin transport quantities, the longitudinal spin current (LSC) and the STT, were compared with those of the underlying spin structures, depending on the magnetization orientation of the SP-STM tip. The magnitudes of the spin transport LSC and STT vector quantities exhibit close relations to charge current SP-STM images irrespectively of the skyrmionic topologies. An important quantity, the STT efficiency, measures the exerted torque on the spins of the skyrmionic structures per unit charge current. Such STT efficiency maps were calculated in high spatial resolution for the first time above topologically different skyrmionic spin textures. A great variation of the STT efficiency depending on the lateral position of the SP-STM tip was found, and regions for large values up to ~25 meV/μA (~0.97 h/e) above the rim of the magnetic objects were identified. [1] An illustration of the calculated tunneling electron quantities is given for a selected skyrmionic object in Fig. 1.

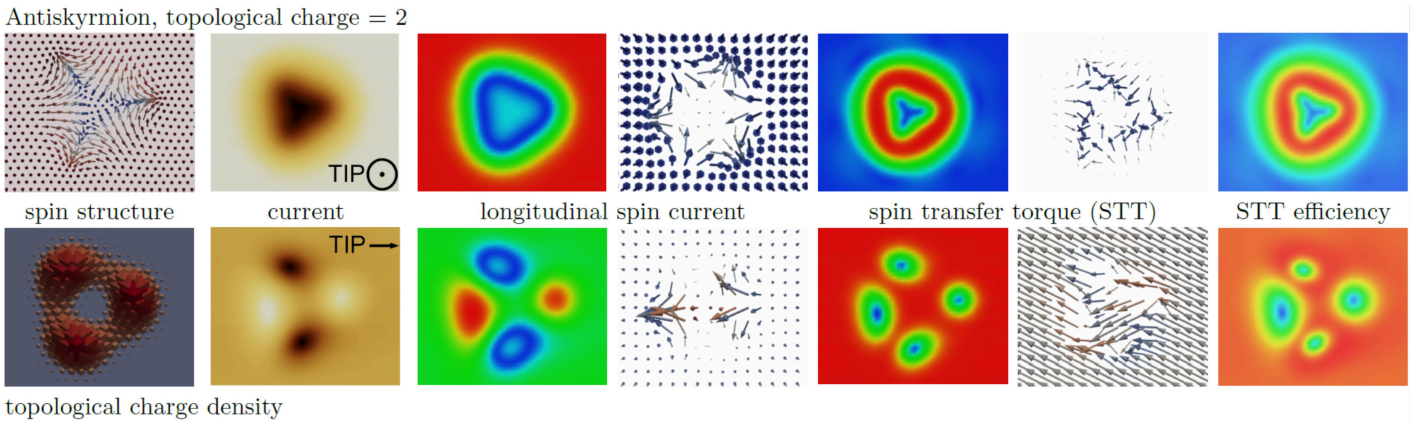

Figure 1. *Summary of the investigated spin transport properties of magnetic skyrmions [1] taking an example of an antiskyrmion with topological charge of 2: The spin structure and the topological charge density distribution are shown together with high-resolution tunneling electron charge and spin transport maps calculated with two types (out-of-plane (1st row) and in-plane (2nd row) magnetized) SP-STM tips: charge current (dark: lower, bright: higher apparent height in constant-current mode), longitudinal spin current (LSC) magnitudes and vectors, spin transfer torque (STT) magnitudes and vectors, and STT efficiency. For the magnitudes of the spin transport quantities blue means lower, and red means higher values. For the vector maps the coloring of the vector components corresponds to red: outward, blue: inward, gray: in-plane.*

Theoretical contributions to various surface science topics — Van der Waals-corrected density functional theory (DFT) calculations were performed in collaboration with a Korean group to examine the initial stages of CuI (p-type transparent semiconductor at room temperature) ultrathin film formation on Cu(111) within the framework of ab initio atomistic thermodynamics. Simulated STM images are in good agreement with experimental results. Moreover, it was found that the surface work function is modulated by a competition between charge transfer and polarization effects, which is determined by the local surface structure. [2]

In collaboration with another Korean group, DFT and STM calculations were employed to investigate the strain-induced structural instabilities between triangular and stripe phases in a pristine single layer NbSe2, and to analyze the energy hierarchy of the structural and charge modulations. The observed wavelength of the charge

modulation is reproduced with a good accuracy in comparison to experiments. [3]
Azobenzene molecular switch has been studied on h-BN/Rh(111) in collaboration with the University of Szeged. Experimental STM indicated a clear preference for trans-azobenzene adsorption in the pores, manifesting a templating effect, but in some cases one-dimensional molecular stripes also form, implying attractive molecule-molecule interaction. DFT calculations provided further details regarding the adsorption energetics and bonding and confirmed the experimental findings. Based on the results, a mechanism of initial azobenzene molecular growth on the h-BN/Rh(111) nanomesh structure was proposed. [4] Furthermore, DFT calculations were employed to study ethanol adsorption and the decomposition product of atomic hydrogen on pristine h-BN/Rh(111), and also on a Au atomic cluster on h-BN/Rh(111). Strong B-H bonds were found in the absence of gold, and larger negative charges on low-coordinated Au atoms were identified responsible for their enhanced catalytic activity. [5]

In collaboration with a Chinese group, we contributed to the extensive DFT study of finding a favorable transition metal center and pathway of electrocatalytic reduction of nitrogen (N_2) for producing ammonia (NH_3) at relatively low overpotential and high selectivity with respect to hydrogen evolution in single-atom catalytic systems on a 2D phthalocyanine molecular layer. Mo was found the best performing transition metal atom for this purpose. Moreover, the dipole of the N≡N triple bond in the adsorbed N_2 molecule was proposed as a better theoretical indicator for predicting the catalytic performance of active sites in the nitrogen reduction reaction. [6]

Degenerate manifolds in the classical antiferromagnet on the fcc lattice — Even though the earliest works on magnetism on face-centered-cubic lattices have been around for almost a century, quite surprisingly systematic study of the classical phase diagram for exchanges going beyond the second nearest neighbour seems to be missing from the literature. Inspired to fill this gap, we performed a detailed study of the ground-state phase diagram of the classical frustrated Heisenberg model on the fcc lattice. We found quite many exciting results on the way. Most remarkably, we identified points in the phase diagram where the ordering momenta form lines and surfaces in reciprocal space, leading to sub-extensive degeneracy in the ground state manifolds. Writing the Hamiltonian as complete squares of spin motifs, we established a link between the real-space and reciprocal-space structures. Large classical ground-state degeneracies may lead to spin-liquid and spin-nematic phases when quantum effects are turned on. We believe that our results will prompt the community to study the more detailed physics of the Heisenberg model in close to these degenerate manifolds [1].

2019

Negative thermal expansion in Cr spinel. — Most materials expand when heated and contract when cooled — this is the usual “thermal expansion”. The higher the temperature, the more the atoms move and the more they stretch the bonds between them, making the material expand. Only in a few exceptional cases does a material display “negative thermal expansion” (NTE), expanding as it is cooled. The water shows such a behavior close to freezing, and this made life on Earth possible.

In a paper published in Physical Review Letters , the international team including a researcher from Wigner RCP explains how the magnetic spinel material $CdCr_2O_4$ expands upon cooling. Experiments on the Chromium spinel $CdCr_2O_4$, carried out by scientists at the High Field Magnetic Laboratory in the Netherlands, reveal that this material also exhibits NTE under specific conditions, namely at low temperatures (below 4K) and high magnetic field (at 30T). This particular property of the $CdCr_2O_4$ is explained by the highly frustrated lattice the magnetic chromium ions form. Besides, there is a strong coupling between the lattice and the magnetic ions, called magnetostriction, which helps the spin to satisfy their magnetic energy at the price of deforming the material. Theoretical calculations show that the frustration and the magnetostriction are the key factors that can translate the heat stored in fluctuations of the spin into contraction of the sample, leading to negative thermal expansion.

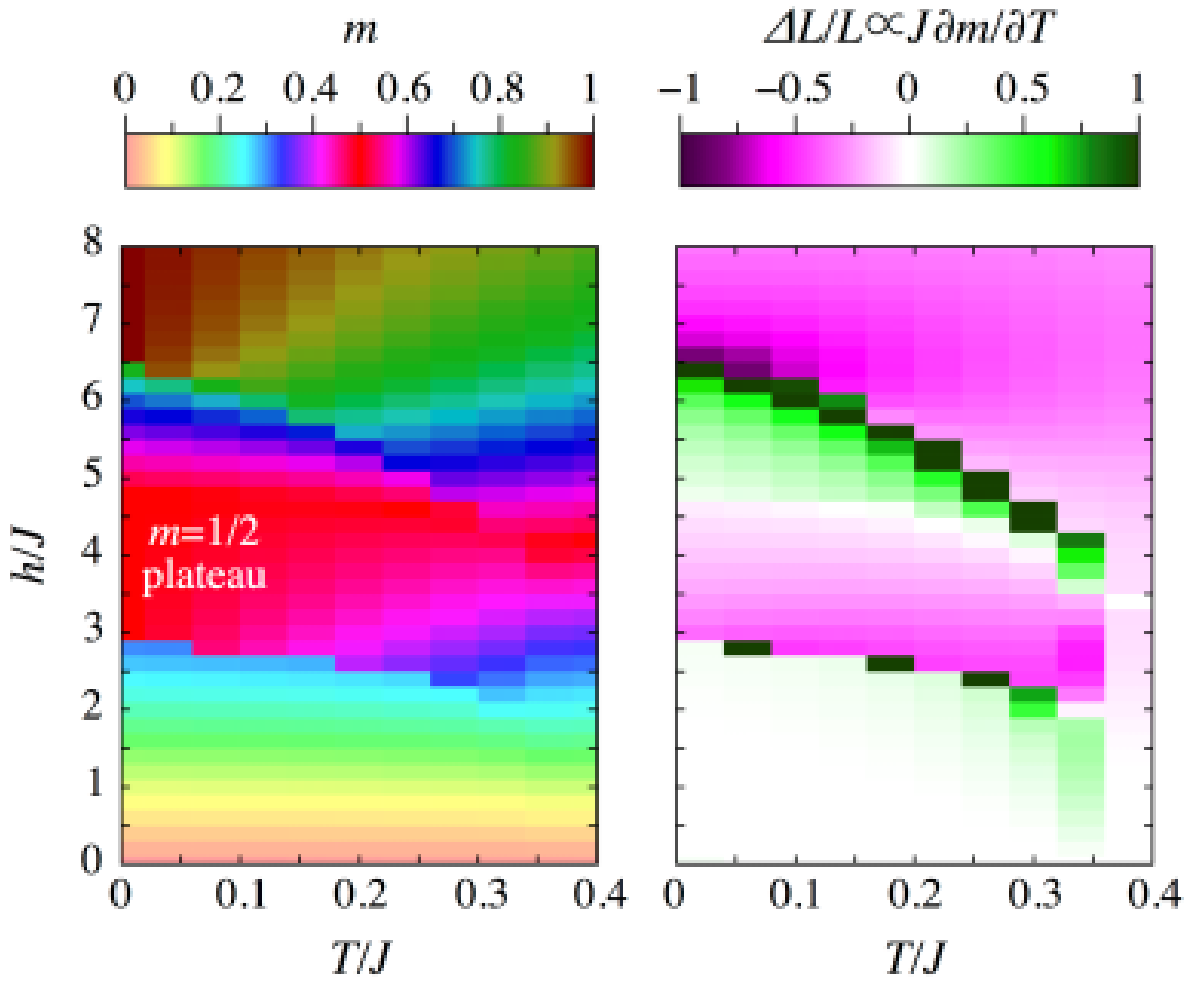

Figure 1. *The magnetization m (left panel) and its temperature derivative (right panel) as a function of magnetic field and temperature. The magnetization is calculated by Monte-Carlo calculations for an effective theoretical model with classical spins and 3456 pyrochlore lattice sites, and is given as a fraction of the saturation magnetization. The negative δm/δT leads to negative thermal expansion ΔL/L in the in the lower part of the half magnetization plateau, and above saturation (L is the linear size of the sample).*

Theoretical contributions to various surface science topics. — The coordination-restricted ortho-site C-H bond activation of 1,3-BPyB and 1,4-BPyB molecules on different metal surfaces (Cu, Au) were studied by a combination of scanning tunneling microscopy (STM), non-contact atomic force microscopy (AFM), and density functional theory (DFT) calculations in collaboration with Chinese and German groups . Ultrathin Mo-oxide films on a Au(111) surface were theoretically studied in collaboration with Korean and Australian groups . The synthesis of N-doped single-layer graphene, doping properties, and doping-induced variation of the local work function of graphene have been investigated on the atomic scale by combining STM/STS, X-ray photoelectron spectroscopy (XPS), and DFT calculations in collaboration with USA, Chinese and Korean groups . The $Cu_2O(111)$ surface has been studied in collaboration with Korean groups using STM and DFT . The magnetic ground states of linear Fe chains with variable lengths on the Re(0001) superconductor surface and the emergence of chiral multispin interactions were reported in collaboration with the Budapest University of Technology and Economics . Adsorbing individual 3d transition metal atoms (Mn, Fe, Co) on the Re(0001) surface, the Kondo coupling, the magnetic anisotropy, and the Yu-Shiba-Rusinov states were investigated depending on the d-band filling of the adatoms in collaboration with German groups .

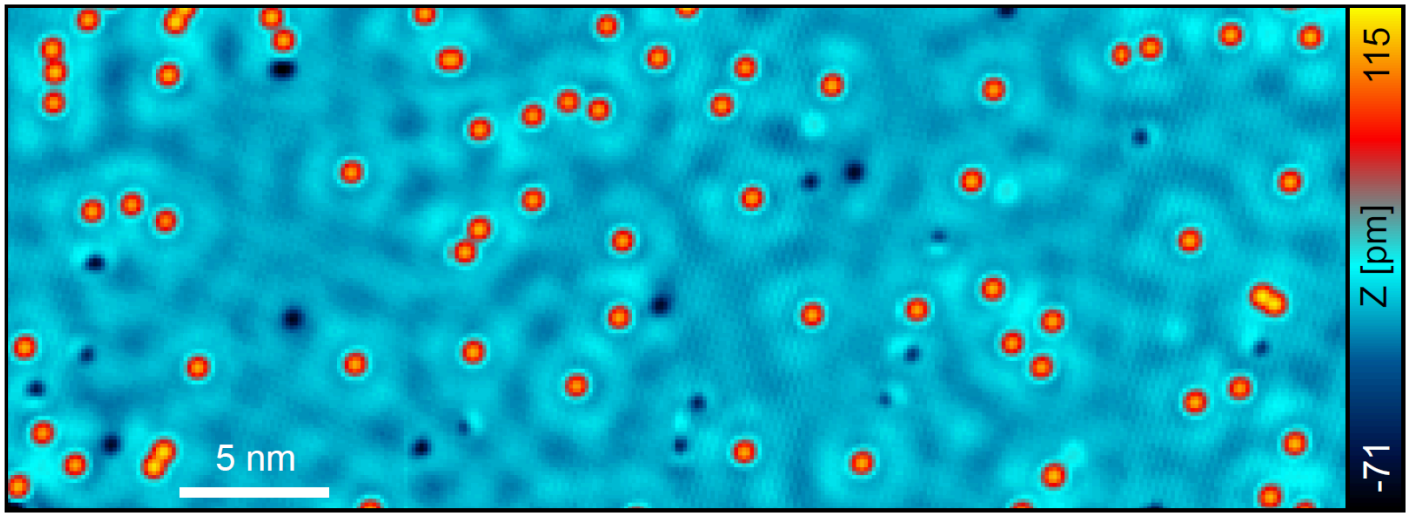

Figure 2. *STM image of Mn atoms on the surface of Re(0001) [7].*

Mixed phase High Entropy Alloys (HEA). — A new formula was worked out, which made possible for the first time to plan the BCC/FCC phase ratio engeneering in the double-phase region of the High Entropy Alloys (HEA). XRD, magnetization and Mössbauer spectra measurements were carried out to study the FCC to BCC phase transformations for 16 new HEA materials based on Mn-Co-Fe-Ni alloys doped with light and heavy sp elements. This phase transformation can be produced in the non-equilibrium, double-phase range of the composition marked by its Valence Electron Concentration between 7,4 and 7,82. It is our conjecture that new materials for magnetocaloric effect can be found between the metastable BCC phases.

2018

Multiferroic materials: During the last few decades, the great potential of multiferroic materials in realizing magnetoelectric memory devices has led to the revival of the magnetoelectric effect and the search for multiferroic compounds. In multiferroics-based memory devices, the writing and reading of magnetic bits by electric field may be realized via the magnetoelectric coupling between the ferromagnetic and ferroelectric orders. However, ferro-ordered phases are extremely sensitive to externals fields. As an alternative approach, information could be stored in antiferromagnetic domains, a concept proposed for metallic compounds in the realm of antiferromagnetic spintronics. We searched whether similar phenomena happen in insulators with coupled antiferromagnetic and antiferroelectric orders. In LiCoPO4 we experimentally demonstrated that the magnetoelectric effect can be exploited not only for the control but also for the identification of antiferromagnetic domains via the strong directional dichroism detected in the THz frequency range -- the absorption coefficients in LiCoPO4 were different for light propagating along and opposite to a given direction in the crystal. Furthermore, we developed a microscopic theory, identifying the main microscopic mechanism behind the magnetoeletric effect, which implies that the same effect arises in other antiferromagnets as well. We expect our study will motivate search for multiantiferroic materials. Moreover, the same principle can also be used for the imaging of antiferromagnetic domains with micrometer resolution in these materials via conventional optical absorption measurements. (Fig. 1).

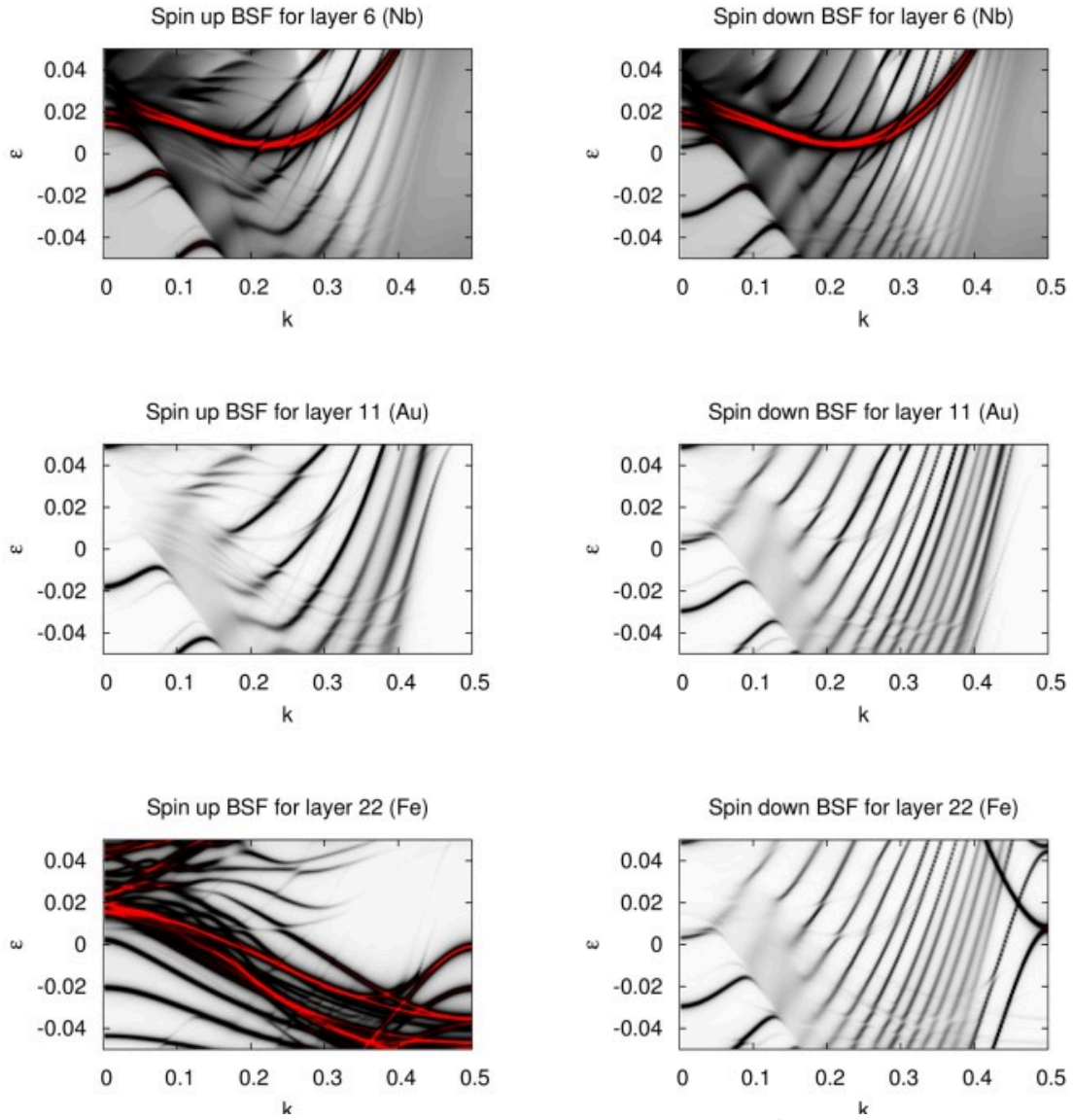

Fig. 1 *Quantum Well states in Fe/Au/Nb(100). Left column is for ↑ right column is for ↓ states. Frist row if for top Nb, middle row for typical Au and bottom row is for typical Fe layer.*

Superconductivity: We have developed a relativistic spin-polarized microscopic theory for realistic superconducting materials which can treat relativistic effects and superconductivity together with spin and orbital magnetism on the same footing.
As an application we have studied Nb/Au/Fe heterostructures where long-period oscillations were found in the critical temperature as a function of the gold thickness and no theoretical explanation existed. We placed different number of Au layers between the Nb and Fe layers, where a face-centered cubic (fcc) growth is assumed for the Au overlayers. While the results show that the Au layers remained non-magnetic, spin-polarized bands around the Fermi level can be observed as shown in the first figure. This is the consequence of the different confinement for the spin-up and spin-down electrons: the spin up electrons are confined in the Au layers only, while the spin down electrons experience a confinement in both the Au and Fe layers. Therefore, due to the different confinement lengths between the spin channels, more bands are observed for the spin-up states than for the spin-down states. Since, the order parameter is influenced mostly by the states in the close vicinity

of the Fermi level, we can conclude that a pairing state (in the Au) can occur between two electrons on the induced split parts of the Fermi surface caused by the quantum well states. Hence, the Cooper pair can acquire a finite momentum leading to the oscillation of the order parameter (analogously to the Fulde–Ferrell–Larkin–Ovchinnikov (FFLO) state). In fact, we found an oscillating behaviour of the order parameter as shown in the right figure. The period of these oscillations depends on the number of Au overlayers since the band structure and the number of quantum well states depends on the thickness of the Au. For thicker Au overlayers as the number of the quantum well states are increasing, the bands in the spin up and spin down channel are separated by smaller and smaller q vectors, which leads to an increase of the period of oscillation as a function of the Au thickness. Our theoretical finding explains the oscillating behaviour of the order parameter and suggests that these Tc oscillations observed in that experiment may also be a consequence of the interplay between the quantum-well states and ferromagnetism.

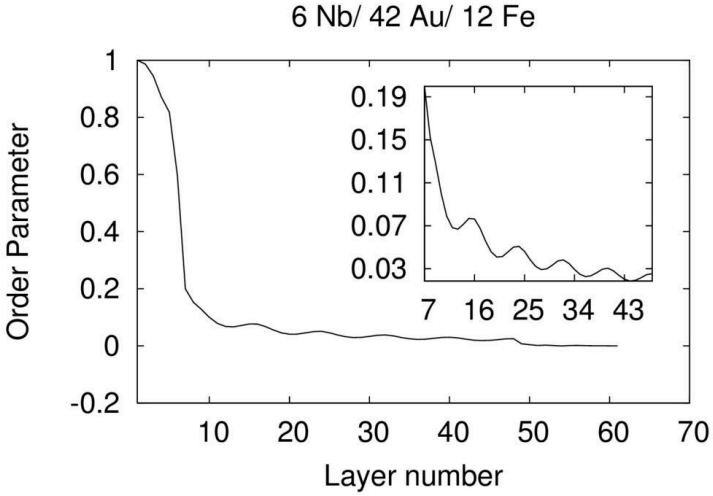

Fig. 2 *Oscillation of the order parameter in Fe/Au/Nb(100)*

High Entropy Alloys: The investigated multi-component high entropy alloys (HEAs) represent a solution for an age-old problem: combination of high strength and high ductility of metallic alloys. In this respect, at present two competing materials are in the frontier of material research:- Nanoscale particle strengthened steels like the old oxide dispersion strengthened (ODS) alloys and the newly developed co-precipitation strengthened steels and - Multicomponent High entropy alloys (HEAs) based on solid solution strengthening. we have followed an integrated computational prediction and experimental validation approach. The computational-aided alloy design was based on first-principles calculations. First, we addressed the forming ability of single-phase HEAs predicting its maximum strength and confirmed the validity of the conjecture about strength (hardness) versus e/a correlation. The theoretical prediction of the elastic properties of various HEAs was contrasted with the available experimental values. Furthermore we studied the twinning as the fundamental mechanism behind the increased strength and ductility in medium- and high-entropy alloys. Second, we dealt with dual-phased HEAs starting from the single-phase NiCoFeCr and adding sp elements like Al,Ga, Ge and Sn. By combining the measured and theoretically predicted temperature-dependent lattice parameters, we revealed the structural and magnetic origin of the observed anomalous thermal expansion behavior [4]. The nanoindentation test revealed a ‘fingerprint” of the two-phase structure. The Young’s and shear moduli of the investigated HEAs were also determined using ultrasound methods. The correlation between these two moduli suggests a general relationship for metallic alloys.

2017

Superconductivity in layered heterostructures. — During the previous years, a novel and unique computer code was developed which allows us to study the nature of the Andreev bound states related to the proximity effect in normal metal–superconductor heterostructures based on the first-principles Bogoliubov–deGennes (BdG) equations. For the first time, we succeeded in applying the SKKR method for solving the Kohn–Sham–Bogoliubov–deGennes (KSBdG) equation which allowed us to investigate the quasiparticle spectrum of superconducting heterostructures. This year, a fully relativistic generalization of the BdG equations within Multiple Scattering Theory has been derived. The method allows the solution of the first-principles Dirac–Bogoliubov–de Gennes equations combined with a semi-phenomenological parametrization of the exchange-correlation functional. The major difficulty during the development was to derive simple conditions for the case when the right-hand-side and left-hand-side solutions must be treated separately while setting up the corresponding Green function. As an application of the theory, we calculated the superconducting order parameter in Nb/Fe and Nb/Au/Fe systems. We found Fulde–Ferrell–Larkin–Ovchinnikov like oscillations in the iron layers, but more interestingly an oscillatory behaviour is observed in the gold layers as well.

Thin Film Magnetism. — Non-collinear magnetic structures have been investigated in ultrathin films by combining ab initio electronic structure calculations with numerical spin model simulations. The experimentally observed significant increase in the spin spiral period as a function of temperature of three-atomic-layer thick Fe films on Ir(111) has been explained. Ab initio calculations revealed how the addition of hydrogen to a two-atomic-layer thick Fe film on Ir(111) leads to the formation of magnetic skyrmions in place of the spin spiral ground state of the pristine system, in agreement with scanning tunneling microscopy measurements. Theoretical predictions have been made on the characterization of skyrmionic structures with various topological charges.

High Entropy Alloys. — Looking for high-strength and high-temperature-resistant high-entropy alloys (HEAs) new refractory HEA compositions have been predicted theoretically bycombining a refractory CrMoW alloy with late transition metals (LTM = Ni, Co, Fe, and Mn). Ab initio calculations revealed that the LTM additions increase the ductility, but reduce the strength of these CrMoW based alloys with single-phase BCC structure.

The magnetization components of permeability spectra for annealed nanocrystalline (Finemet) core have been studied and four contributions have been revealed for the first time in the literature: i) eddy current; ii) Debye relaxation of magnetization rotation, iii) Debye relaxation of damped domain wall motion and iv) resonant type DW motion. Although the relative weight of these contributions changes with the frequency and exciting field amplitude, the role of eddy current cannot be neglected even for the smallest applied field. These components can be found in the powder cores of soft magnetic composites as well.

Observation of spin-quadrupolar excitations in Sr2CoGe2O7 by high-field electron spin resonance. — When we think of a spin, usually we imagine an arrow pointing somewhere (representing the expectation values of the components of the spin operator), and with the arrow we associate a magnetic moment. Upon time reversal, the arrow reverses its direction. This is a reasonable picture for the spin 1/2 of the electron, but for larger spins this does not exhaust all the possibilities. For example, the dimension of the Hilbert space is 3 for the spin 1, and we can construct spin states for which the expectation values of all the three spin operators vanish — the state does not point anywhere, it cannot be represented by an arrow. The simplest example is the 0 eigenstate of the S2 operator. In fact, there are three linearly independent such states (the zero eigenstate of the Sx, Sy and Sz operators), spanning the Hilbert space. Though they cannot be represented by an arrow, they still break the rotational symmetry, since quadratic forms of spin operators differentiate among them. Instead of arrows, we can use directors (like in the case of liquid crystals), as the rotation by π around an axis perpendicular to the director returns the same state (up to a phase factor). These states are called spin-quadrupoles. Furthermore, these states do not break the time-reversal symmetry.

Similarly, the long-range-ordered states of interacting spins are usually time-reversal-breaking states, with a configuration of “arrows” that repeats itself on the lattice. However, under favorable conditions, interacting spins can produce ordered states where the order parameter is of spin-quadrupolar character which does not break the time reversal symmetry. Theoretically, such phases have been established in spin-one Heisenberg models extended with higher-order spin interactions. Even more interestingly, time-reversal invariant ordered states can also be realized in spin-1/2 systems, where the quadrupole-like order parameter is distributed between two spins on a bond, leading to a so-called nematic ordering.

These theoretical developments have inspired the quest to nematic and quadrupole phases in real materials. However, when relying on standard experimental methods, such phases usually remain hidden. Most of the experimental probes detect spin-dipolar (ΔS=1) transitions, and they do not interact with the spin-quadrupoles, as their detection requires ΔS=2 transitions.

In a collaboration with experimental researchers from Osaka University, we found an unambiguous experimental observation of spin-quadrupolar excitations in the layered Sr2CoGe2O7 multiferroic compound. In this compound, the Co ions are in the centers of tetrahedra formed by the four surrounding O ions (Fig. 1). Since the inversion symmetry is absent, the relativistic spin-orbit coupling allows the coupling of the electric polarizations to the spin-quadrupolar operators. Due to this magnetoelectric coupling present in the Sr2CoGe2O7, the non-magnetic, purely spin-quadrupolar excitation becomes electrically active and detectable by electromagnetic waves, like the electron spin resonance spectroscopy.

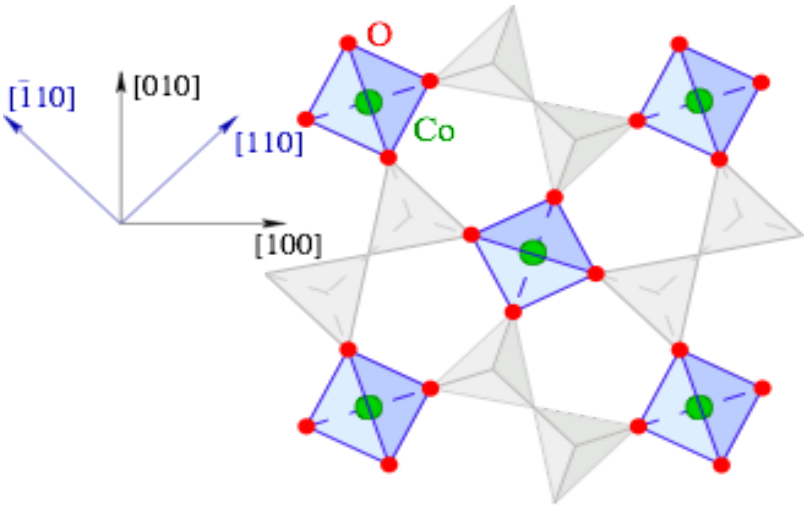

Figure 1. The schematic crystal structure of the Sr2CoGe2O7 multiferroic compound projected onto the ab plane. The green spheres represent the magnetic Co2+ ions with S = 3/2 surrounded by four O2− ions (red) in an alternating tetrahedral environment.

In the electron spin resonance spectra of Sr2CoGe2O7 above the saturation field of 20T, a mode with twice the g-factor of the usual modes is observed (Fig. 2). This indicates the absorption of two magnons, just what is needed for the creation of a quadrupole wave. Indeed, we could explain the features of the experimental spectra taken in different geometries by a simple theoretical model of the spin-quadrupolar wave providing not only a qualitative description, but also a quantitative agreement.

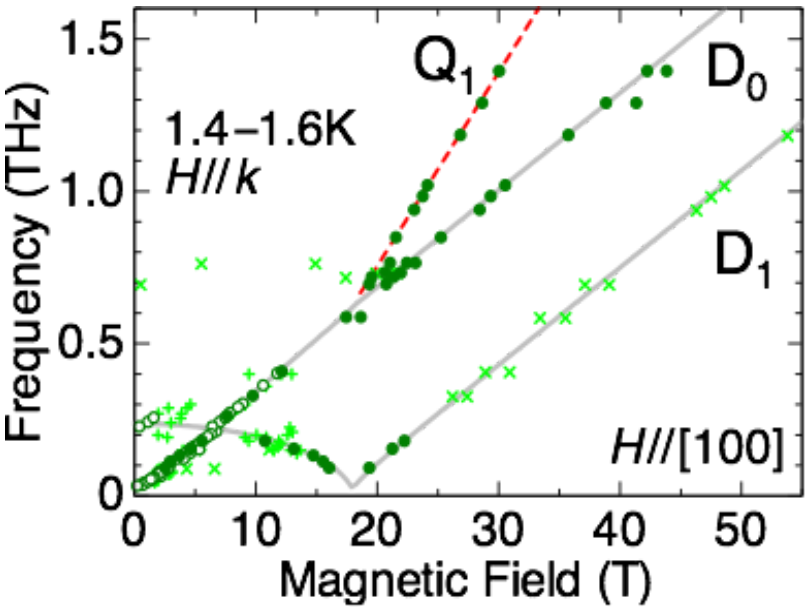

Figure 2. Frequency-field diagrams of the ESR resonance fields of Sr2CoGe2O7 for magnetic fields parallel to the [100] direction of the external magnetic field. The solid lines represent the dipolar resonance modes from the multiboson spin-wave theory. The red dashed line indicates a resonance mode with a slope twice larger than the others, corresponding to a two-magnon excitation — the quadrupolar mode.

The most significant point of our finding is the first observation of non-magnetic spin-quadrupolar excitation in an antiferromagnetic material (Fig. 3). Such quadrupolar degrees of freedom become inherent in systems with larger than S=1/2 magnetic moments, regardless of the presence of magneto-electric coupling. Upon condensing such multipolar excitations, magnetically disordered exotic quantum phases may arise. The experimental identification of quadrupole excitations with vanishing gap gives us a possibility to identify long-sought nematic phases, which stand without any usual magnetic fingerprint and are almost impossible to tell apart from other non-magnetic phases. Furthermore, our work will stimulate the application of the magnetoelectric effect as a spectroscopy tool.

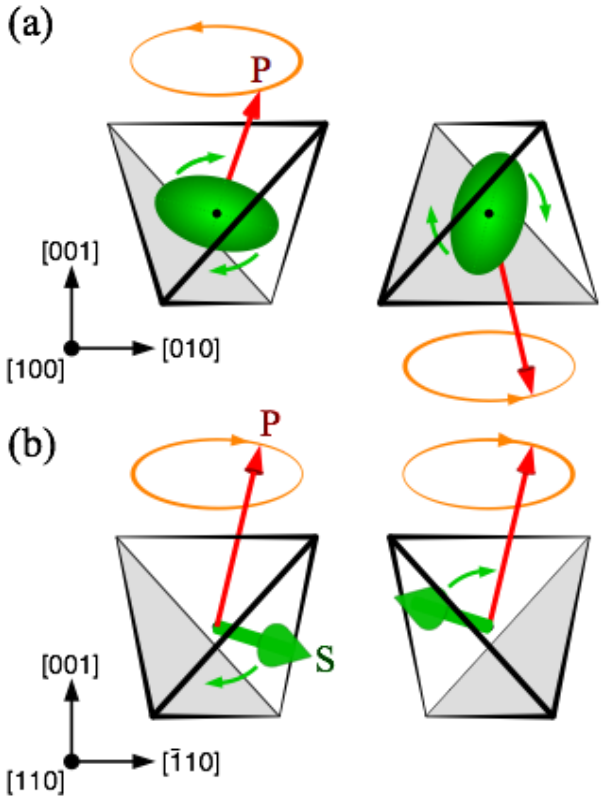

Figure 3. Schematic plot of (a) the Q1 quadrupolar mode for H∥[100] and (b) the dipolar modes for H∥[110], as seen from the direction of the magnetic field. In both cases the oscillating component of the uniform electric polarization P (shown by orange ellipse) is perpendicular to the external magnetic field H, therefore they are active in the Faraday configuration. The green ellipse represents the rotating quadrupolar moments, while the green arrows the precessing dipolar spins on the two sublattices. The red arrows show the electric polarization vectors which are excited by the oscillating electric field.